University of Louisville

ThinkIR: The University of Louisville's Institutional Repository

Electronic Theses and Dissertations

1-2021

Wetting and drying dynamics for TiO2 with PbS quantum dots.

Kelly M. Lee
University of Louisville

Recommended Citation

Wetting and Drying Dynamics for TiO$_2$ with PbS Quantum Dots

By

Kelly Marie Lee

B.S. University of Louisville 2018

A Thesis

Submitted to Faculty of the

J.B. Speed School of Engineering of the University of Louisville

For the Degree of

Master of Engineering

In Chemical Engineering

Department of Chemical Engineering

University of Louisville

Louisville, Kentucky

July 2021

Wetting and Drying Dynamics for TiO2 with PbS Quantum Dots

By

Kelly M. Lee

A Thesis Approved on

July 30 2021

By the following Thesis Committee

Gerold Willing Digitally signed by Gerold Willing
Date: 2021.08.09 12:49:58 -04'00'

Thesis Chair

Thesis Co-Chair (if applicable)

Vance Jaeger Digitally signed by Vance Jaeger Date:
2021.08.09 11:54:58 -04'00'

Committee member

Stuart Williams Digitally signed by Stuart WilliamsDate:
2021.08.09 12:05:31 -04'00'

Committee member

Committee member

ABSTRACT

Wetting and Drying Dynamics for TiO$_2$ with PbS Quantum Dots

Initial solar cells utilized silicon and alloys for their economic viability. Photoelectrochemical photovoltaic cells were discovered with technological advancement which increased solar efficiency and further improved economic feasibility leading to quantum dot sensitized solar cells. Lead sulfide quantum dots and titanium dioxide were studied for wetting and drying effects. Zeta potential, pH values, SEM, and optical microscopes quantified or observed the colloidal suspension and dried sample behavior. Combined mixtures of lead sulfide and titania were dried at 3.6 pH and 12.56 pH values. This due to the observed zeta potential isoelectric point of titania, and behavior showed increased stability occurring for those pH values, respectively. SEM imaging was optimized to achieve a thin layer of dried material. Lab microscope imaging further confirmed what was occurring in SEM imaging; the materials were falling out of suspension with lead sulfide settling to the bottom (black or grey material) and titania (white) on the top surface of the dried droplet at both pHs.

This work completed further establishes behavioral evaluation of individual materials related to creating third generation solar devices made with quantum dots verses that of current materials used for second generation materials like CdS, CdSe, and CdTe. This work contributes to general knowledge of material characteristics of lead sulfide as a nanoparticle as a potential quantum dot in a titanium dioxide microparticle system.

ACKNOWLEDGEMENTS

Contents

NOMENCLATURE

U_e electrophoretic mobility, m2/V * s

V_e electrophoretic velocity, m/s

ε_{rs} relative permittivity of the electrolyte solution

ε_0 electric permittivity of the vacuum

η viscosity

E external applied field

P_D Disjoining Pressure, N/m^2

A Surface area of interacting surface, m^2

G total Gibbs energy of the interaction of the surfaces, J

X is the distance in meters

A, V, T indices are surface area, volume, temperature, remain in constant with the derivative of the total gibbs free energy of the interactions between the two surfaces with respect to the distance

P_T is the total pressure in a film

P_o pressure in the bulk of the same phase of the film

A_H Hamaker constant, J

δ_0 liquid film thickness in meters

TABLE OF FIGURES

LIST OF TABLES

INTRODUCTION

Background and Applications

Quantum dots as a technology are used in a variety of sectors and the applications continue to be researched as far as solar applications. The versatility of quantum dots has impacted medical imaging, LEDs, thermoelectric, and transistors. The production of the quantum dots (QD) industry is estimated to reach 35 billion dollars by 2030 (NPR Newswire, 2020) which has become attractive to recognizable consumer companies like Hewlett Packard and Samsung.

QDs are comprised of semiconductor nanoparticles that are used to create these bodies which can both absorb energy and emit light. There are three main types of quantum dots: core-type, core-shell, and alloyed. Core-type have uniform compositions and have photoluminescent and electroluminescent properties. Core-shell QDs are known for their unique optical properties. The shell located on the outer edge of the core, specifically, improves the overall stability and photoluminescence. Alloyed QDs can be manipulated to enhance optical as well as the overall electronic properties. Alloyed QDs can maintain crystal size; they allow for compositional and structural changes. For the purposes of this investigation, core-type nanoparticles in a liquid medium are the focus (Sigma Aldrich, n.d.).

Purpose

This work investigates the effects of drying methods on the overall structure and therefore viability of structures that are stabilized by nanoparticle haloing. Titanium dioxide is used in dye sensitized solar cells and is a reliable, energy efficient, and safer

9

alternative to previous solar cell materials. Studying quantum dots with this system are beneficial to understanding a third-generation system that allows for customization with band gaps. Lead sulfide is highly tunable and understanding how to better utilize this property is vital to properly developing higher efficiency solar cells. To add, the impacts of this knowledge help elucidate the specific effects of the drying dynamics which have not been studied at length for the lead sulfide and titanium dioxide system. As a project, it contributes to understand the drying behaviors of these materials and how the suspension measured via zeta potential affects the drying dynamics.

Literature Review
Quantum Dots, Microparticle, and Nanoparticle

The first approach was researching different types of quantum dots by casting a wide array looking for various species that have been studied under the assumption of similar chemical properties and processes for making QDs. QDs have gained relevance related to the photovoltaic market recently as technology has been developed to replace materials for economic viability, safety of materials, and increased efficiency. In the photovoltaic market, there are three common classifications: first, second, and third generation devices. These are categorized by their technological properties and characteristics (Kouhnavard et. Al., 2014).

First generation devices are single or multi-crystalline and are made of silicon. This category is 85% of the market and typically have an efficiency of 20%. The challenges with first generation devices are the material cost, high manufacturing temperatures, quality requirements for silicon, and the environmental impact. Second generation (15% of market) devices are cheaper and less efficient thin inorganic films and typically made of cadmium telluride. Third generation devices require increased

efficiency and cheaper production cost. Third generation devices include dye-sensitized solar cells, quantum dot-sensitized solar cells, and organic solar systems. With efficiency of dye-sensitized solar cells established, innovations related to inorganic semiconductors, like quantum dots, are being studied (Kouhnavard et. Al., 2014).

The unique characteristic of quantum dots is their customizable nature as far as band gaps to harvest different wavelengths of light. The disadvantage of QDs is their lower efficiency comparable to dye sensitized solar cells regarding electron loss from interfacial surfaces; this includes interfaces between particle layers of the solar cell as well as between the electrolyte and particles with respect to both the electrode and counter-electrode.

Optical Properties
As a quantum dot absorbs light, electrons becoming excited. This leads to an electron reacting and jumping a conduction band. When this phenomenon occurs, it leaves a hole behind. When an electron and a hole bind, it forms an exciton. Whenever the electron returns to the original state, the energy released is in the form of light known as fluorescence. While this is not related directly to the scope of this project, it directly contributes to the understanding of quantum dots and their properties as nanomaterials.

Zeta Potential
Zeta potential is the electrokinetic potential of a colloidal fluid and measures at the slipping plane. The slipping plane is where the edge of the diffusive layer on the particle and the surrounding liquid meet. The diffusive layer located around the particle surrounds the stern layer and finally the particle. Zeta potential is measured in millivolts (mV) by a zeta potential analyzer. The typical behavior of the system falls in an absolute

scale, meaning it disregards whether the charge is measured to be positive or negative. The zeta potential describes the stability of the suspension (Raja & Barron, 2021). As shown in Table 1 below, the target is to achieve a decent stability with our solution, which depending on pH is either nitric acid or potassium hydroxide.

Table 1. Zeta potential with corresponding behavior in solution

Zeta Potential (mV)	Behavior
0 – 5	Flocculation
10 – 30	Incipient
30 – 40	Moderate
40 – 60	Good
61+	Excellent

Nanoparticle Haloing

Nanoparticle haloing describes what ideally would be occurring in this mixture of lead sulfide and titanium dioxide. Haloing occurs when a microparticle is surrounded by charged nanoparticles that create an electrostatic repulsion between the larger particles (Tohver et al., 2001). With a proper pH, concentration of microparticles to nanoparticles, and a decent zeta potential charge of at least 30 mV, for a colloidal suspension can be stabilized through nanoparticle haloing. In this case charged particles surround the microparticles and would stay in an equally distributed suspension as the material dries as in Figure 1 below.
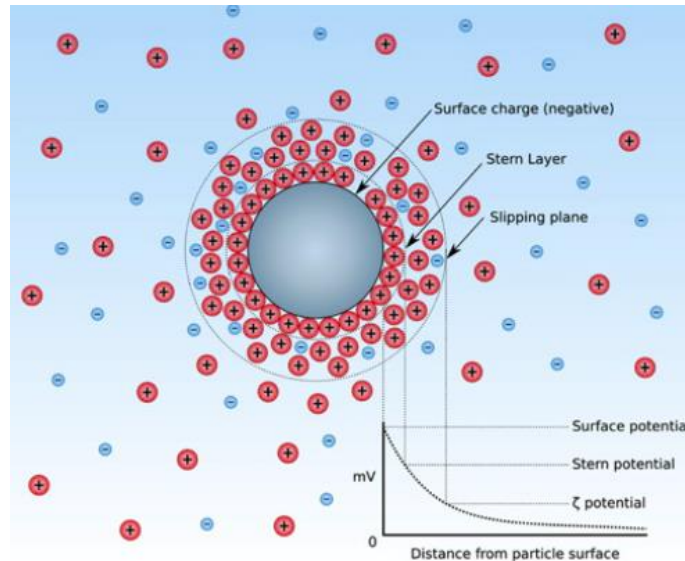
Figure 1. Nanoparticle haloing concept diagram (Raja & Barron, 2021).

In Figure 1 above, is a schematic representing the layers created by electrical potential at the slipping plane known as nanoparticle haloing. In the case of nanoparticle haloing in this study utilizes a base microparticle of titanium dioxide with the nanoparticles being lead sulfide. Ideally when assessing if the material dried in suspension, imaging through a scanning electron microscope and a standard lab microscope should create observable images to understand the stability and temperature effects on the colloidal suspension (Raja & Baron, 2021).

Quantum Dots and Solar Application

Lead sulfide and titanium dioxide in these colloidal suspensions are conductive particles that can be used in solar cells. While PbS is used in this system, a variety of quantum dots (CdS, CdSe, CdTe) can be used and PbS is less typical than other types of quantum dots. The ideal overall structure of a solar cell using titania and PbS quantum dots is show in the Figure 2 below.
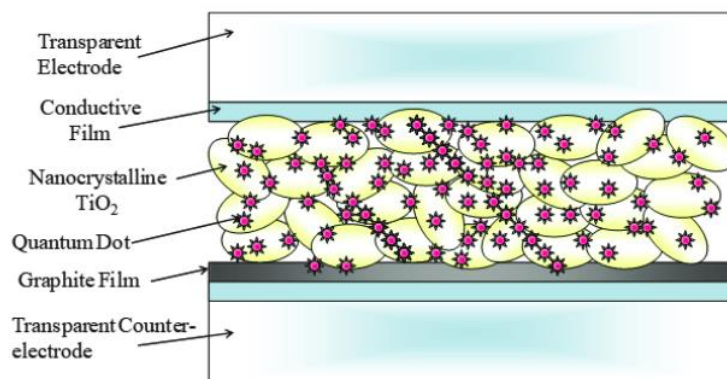
Figure 2. Lead sulfide QD solar cell diagram *(Jasim, 2018)*.

The overall operation occurs as depicted in the schematic in Figure 3 below. QDs are excited from the ground state by photon absorption. The result of photo absorption results in an exciton. The energy (photon) is absorbed by the conduction band of the titanium dioxide that results in an oxidation reaction.

Dissociation of excitons occur if thermal energy exceeds its binding energy (Jasim 2018). The electron is injected into the conduction band of the bandgap of the titanium dioxide thin film resulting in the oxidation of the quantum dots. The same electron is transported through the layer and is delivered as electrical energy via the counter electrode.

The electrolyte, in this case iodine, acts as a reoxidation ions and plays a role in between titanium microparticles and the counter electrode. The quantum dots are regenerated by the electrolyte, iodine ion, which places the quantum dot back to the ground state. Then the iodine ion returns to its triiodide ion state. As it returns to this state, the ion encounters the counter electrode which then returns to a single iodine ion (Jasim, 2018). This is represented in Figure 3 below.

14
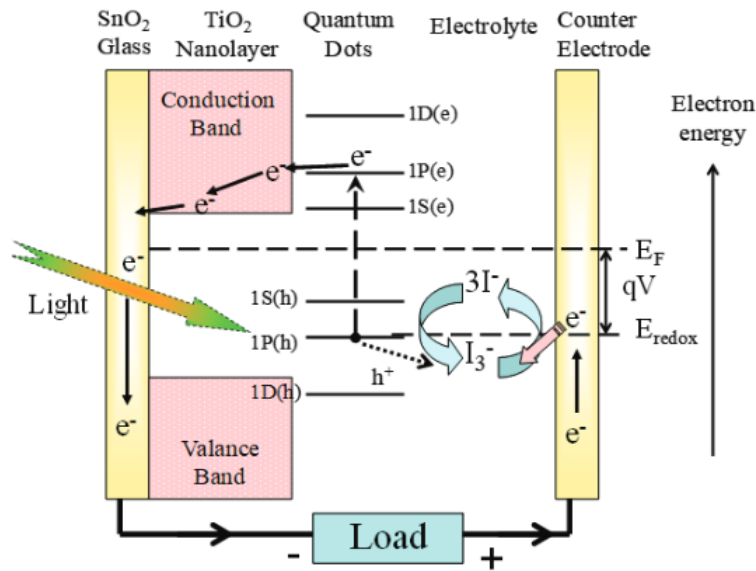
Figure 3. Schematic of movement across QD solar cell (Jasim, 2018).

A QD solar cell using lead sulfide would utilize glass substrate (Indium Tin Oxide (ITO) or Fluorine-doped Tin Oxide (FTO) glass), with PbS quantum dots and titania as similarly depicted in Figure 2. The electrolyte would likely be triiodide solution that is already used for dye sensitized solar cells. In constructing solar cells, drying the lead sulfide/titanium, and triiodide layers are required to adhere to the FTO/ITO glass surface. A potential counter electrode would be graphite.

One of the most challenging aspects related to drying dynamics of colloids for solar cells currently is the lack of work published to further understand how spreading and evaporation of nanofluids occurs related to structure. What drives this research project is the understanding of drying if a colloidal suspension will behave according to current understanding of wetting and drying dynamics (Harikrishnan et al., 2017). Another layer of complexity to add to the understanding of drying dynamics related to

colloidal suspensions is how drying at different temperatures would affect the droplet's dynamics and dried structure which led to this project.

The goal of this study is to gain further understanding of a nanoparticle haloing system and drying these materials; Theoretically, the potential structure needs to be identified. The ideal nanoparticle haloing structure would occur at the isoelectric point of titania. In this system, the materials would dry while maintaining in suspension with lead sulfide nanoparticles. One factor to consider when discussing these particles in suspension is the depletion interactions. Depletion interactions could hinder the nanoparticle haloing system from forming; particle sizes that are bigger than the target lead sulfide size will interfere with charging to the surface of titania. Another source of error could result from the pressure forces in the droplet. While drying, a titanium particle would be surrounded by quantum dots and as the material crystallizes it develops interstitial sites. With nanoparticle haloing, it is the aim to create a crystal structure that has minimal defects. Defects arise from particles inhabiting spaces that they typically do not inhabit. Part being if there are too many interstitial defects, it will result with the crystal structure collapsing or partially collapsing (Averill & Eldredge, 2019).

Theory
Wetting & Drying Dynamics
The relationship between intermolecular forces influences the overall form of a droplet and drying. Hydrodynamics and Van der Waals forces dictate the formation of a droplet and the drying shape. Disjoining pressure plays into wetting dynamics and is a multicomponent system that includes dispersion, electrostatic forces between materials,

and effects of the solvent. Disjoining pressure via attraction between two surfaces can be expressed as equation 1:

$$P_D = -\frac{1}{A}\left(\frac{\partial G}{\partial x}\right)_{T,V,A} \qquad 1$$

This includes surface area, and the entropic nature in relation to films related to the liquid-vapor interface. A is the surface area of interacting surface in squared meters. The second term is the partial derivative of total Gibbs free energy of the interaction of the surfaces with respect to the interface length, x. A, V, and T indices are surface area, volume, temperature, which remain constant with the derivative.

The combination of forces leads to equation 2 below. P_T is total pressure in the film which is the combination of P_D, the disjoining pressure, and P_o, pressure in the bulk of the same phase of the film.

$$P_T = P_0 + P_D \qquad 2$$

Changes in these factors as well as when colloids start to establish structure increases the overall pressure via structural pressure. As film thickness increases, the overall forces decay and vary over time. Enhanced pressure leads to the spreading of the droplet as the colloidal droplet begins to dry, in this case, on a flat surface which can be represented as equation 3. A_H represents the Hamaker constant and δ_0 the liquid film thickness in meters. The Hamaker constant represents the van der Waals interaction relating term for disjoining pressure.

$$P_D = -\frac{A_H}{6\pi\delta_0^3} \qquad 3$$

Nanoparticles and their contribution to decay during drying is related to their size and type, and interactions can vary between substrate, base, and adsorbed nanoparticles. Decay of structure is dependent on surface tension and viscosity. Surface tension related to nanofluids increases with both increased concentration and particle size. Viscosity increases as nanoparticle size decreases and is dependent on the material itself. Smaller nanoparticles show more change as far as structural decay (Bhyiyan, et al., 2015).

Drying of these suspensions and the resulting structures are also dependent on the pH related to zeta potential. Depending on the pH, the charge of the materials can determine the stability of a solution and how long the materials will stay in suspension. If two materials are both negatively or positively charged, the materials will repel each other. If of opposite charges, materials should stay in suspension given the optimal pH range. Related to drying dynamics, if the materials in suspension are repelling each other, nanoparticle haloing will not occur and there will be two distinct layers that form. As a droplet dries, coffee ring type structures will form. The ring structure develops from diffusion and convection occurring. Convection evaporates the liquid and diffusion of materials in the droplet. This relationship between convective and diffusive forces can be quantified by the Peclet number (Pe). For high values, materials will accumulate into two layers. For low Peclet values, the particles are uniformly dispersed (Osman et. al., 2017). If fully suspended and nanoparticle haloing does occur while drying, ideally QDs would be distributed in the droplet side profile view.

Suspension related to Zeta Potential

Zeta Potential is calculated via electrophoresis which is the movement of colloidal particles that happen to be charged in a liquid media when an electrical field applied to the system. This is expressed in two equations for electrophoretic mobility and electrophoretic velocity as shown below in equations 4, 5, and 6. The variables U_e and V_e represents the electrophoretic mobility and velocity, respectively. Permittivity values, ε_{rs} and ε_0, are the relative permittivity of the electrolyte solution, and the electric permittivity of the vacuum. η is viscosity. E is the external applied field and of course, ζ is zeta potential (Raja & Barron, 2021).

$$u_e = \frac{\varepsilon_{rs}\varepsilon_0\zeta}{\eta} \qquad\qquad 4$$

$$v_e = \frac{\varepsilon_{rs}\varepsilon_0\zeta}{\eta}E \qquad\qquad 5$$

$$v_e = u_e E \qquad\qquad 6$$

Scanning Electron Microscope (SEM)

SEM is a method of imaging samples that need to achieve higher magnification to assess topography, morphology, composition, and crystallography. Topography is the surface features and is directly related to the material properties of the sample. Morphology is the size and shape of materials in a sample; this directly ties to both material properties and structures. Composition is the material amounts in a sample. The images present a representation of what is occurring as the electrons bounce off the materials. Therefore, it is not considered a true image of a sample but a measured

and calculated image which can be subject to question. Sometimes shadows, misalignment with detector, or organic matter can distort an image that could give inconclusive results (Electron Microscopy, n.d.).

MATERIALS & METHODS

Materials Overview

Lead Sulfide nanoparticles

Lead sulfide nanoparticles were made in the lab using a colloidal synthesis method that is discussed in methods part of this section. Lead sulfide is the nanoparticle of this nanoparticle haloing system and acts as the particle that charges to the microparticle, titania. Lead sulfide was chosen based of the versatility of the material for quantum dots. Lead sulfide is highly tunable and understanding how to better utilize this property is vital to properly developing higher efficiency solar cells. This material appears to be a fine black powder. Lead sulfide was chosen because, it was believed from previous students to be stable in suspension around titanium dioxide's isoelectric point. This bulk material has a charge of 2+.

Zeta Potential Analyzer

Lead sulfide nanoparticles were first assessed based on zeta potential and the overall acidity and basicity of the solution. In the measurements established in the tables below the data points closer to the isoelectric points vary because, the solutions are not stable and therefore leading to measurement errors. In Table 2 below, zeta potential was precisely close to its isoelectric point until the pH increased as the solution became more basic. These data results are acquired on the same sample 5 different

20

times. Each time the instrument resets before performing another run. Figure 4

graphically represents the behavior of lead sulfide materials across pH values while

measuring zeta potential. While the measured zeta potentials of the suspensions are

treated as absolute values, these nanomaterials are negative in charge. Having a

negative charge, lead sulfide particles' behavior will affect the overall behavior of

system (in this case, individual interactions that occur between nanoparticles and

microparticles). The stability of this material is not as expected. Lead sulfide particles

were expected to be higher around 3.6 pH. Therefore, the material's behavior needs to

be assessed on a few different fronts. First, if the particle size is small enough for the

nanoparticle haloing system. With larger particle size, the material will maintain in

suspension at a higher pH than documented. Another factor to consider is if the

surfactant that clumps the lead sulfide particles together potentially is affecting the

overall charge of the material and the zeta potential characteristics.

Table 2. Lead Sulfide zeta potential results in mV at different pHs

Lead Sulfide Zeta Potential								
	pH							
Run	*0.89*	*2.24*	*3*	*4*	*5*	*7*	*9*	*12.56*
1	-13.29	-16.97	-13.55	-14.22	-16.83	-6.83	-33.06	-33.85
2	-10.44	-8.84	-14.22	-15.12	-13.24	-5.71	-33	-35.53
3	32.91	-12.96	-19.57	-10.31	-10.11	-16.36	-34.89	-22.42
4	53.09	-11.3	-18.79	-22.06	-15	-16.55	-28	-39.79
5	-19.89	-14.81	-15.81	-18.27	-12.5	-9.12	-31.09	-27.26
Mean	**8.48**	**-12.98**	**-16.39**	**-16.00**	**-13.54**	**-10.91**	**-32.01**	**-31.77**
Standard Deviation	32.49	3.13	2.69	4.42	2.54	5.21	2.61	6.90
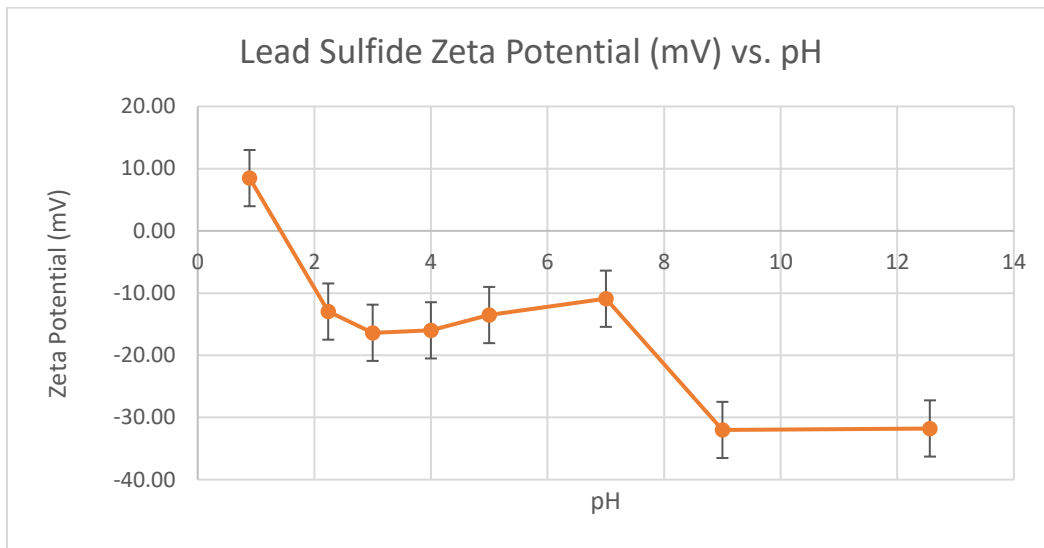
Figure 4. Graphical representation of mean zeta potential(mV) at different pHs. Graphed with one standard deviation error.

Particle size analyzer and SEM

The particle size characterization does not confirm the desired product required to complete the experiment; lead sulfide particle size should confirm it is the nanoparticle in the system. Using this practice of characterizing size of particles is not always accurate. In Table 3 measurements are effective diameter and half width. Effective diameter is the average diameter of the particles. Half width is the statistical distribution width. The instrument can read a minimum of 10 nanometers in diameter, the particle sizing instrument reads closer to that of 20 to 50 nanometers. Error associated with the particle

size analyzer includes the values for half width specifically. Since powders consist of a variety of effective diameters; some are larger and some smaller. The half width or measurement of standard deviation of particle diameters has some level of inaccuracy. Specifically, the first run has a half width that is so low compared to the five runs that it must be an outlier. Rejecting the effective diameter is not necessary because that is the average particle diameter and is still relevant to the data set. While it is still a lower particle diameter than the other measurements, it still could represent smaller particles. Lead sulfide measurements were confirmed via scanning electron microscope as another method.

Lab-made nanoparticles need to be assessed for particle size and characterized for the sake of ensuring the particle size of the quantum dot does not equal or exceed the size of the titanium particles. While the target size was 9 nanometers, the particle size will be a larger range of particle sizes which is characterized in both the larger diameters from the PSA as well as the range of particles captured by the SEM. SEM found larger particles and smaller (closer to 9 nm) in Figure 5 and Figure 6, respectively.

Table 3. Particle Size Analyzer results of lead sulfide. Measuring effective diameter and half width.

Lead Sulfide Particle Size Analyzer Results		
Run	Eff Diameter(nm)	Half Width (nm)
1	323.4	22.9
2	353.9	174.8
3	356.2	177.8
4	525	343.9
5	756.7	467.9
Mean	463	237.4
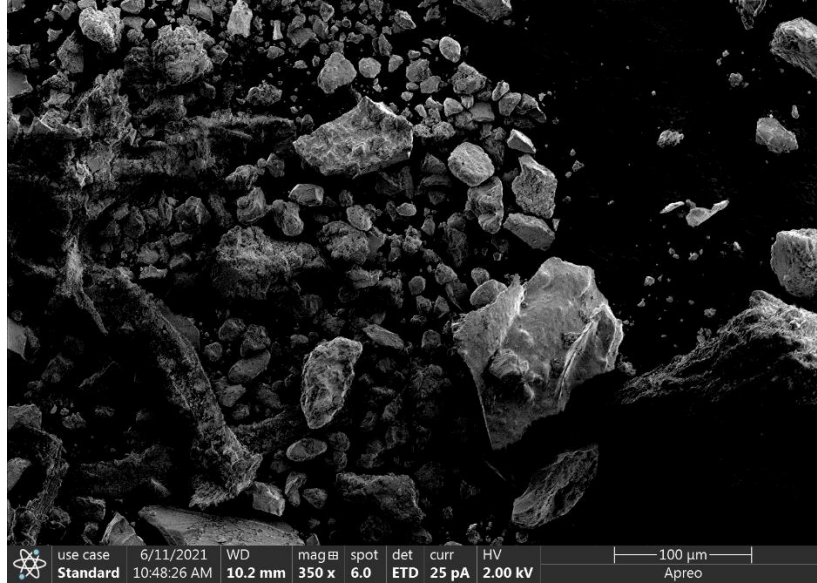
Figure 5. Lab created lead sulfide imaging results using scanning electron microscope (SEM)
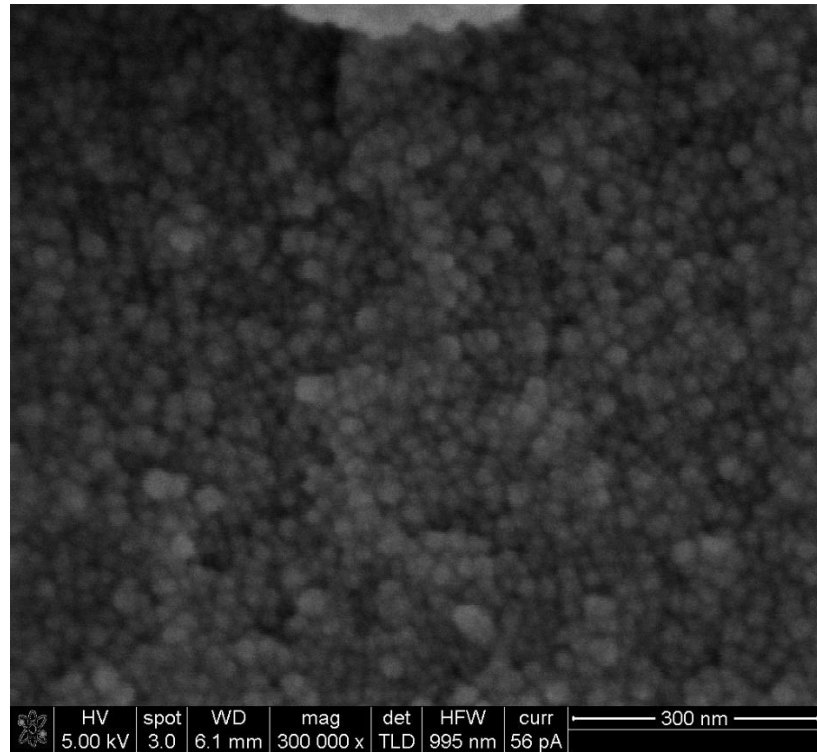
Figure 6. Lead sulfide smaller particles existing in the sample using SEM.

Titanium Dioxide microparticles

Titanium dioxide was ordered from US Research Nanomaterials, Inc. with an average particle size of 800 nanometers. Titanium dioxide's appearance is fine white powder. Documentation provided for this material does not mention the distribution of particle sizes, but this can be confirmed via the statistical distribution width. While Table 5 below shows an effective diameter greater than 800 nm, it must be considered that the zeta potential analyzer/particle size analyzer is not entirely correct or is not able to read this material accurately. Clumps and multiple particles clinging to each other can explain the large particle size measurements that represent double the diameter reported on the product description. Titanium dioxide is also known as titanium (IV) oxide or titania and is classified as the microparticle in the system. Titania is found in consumer products including cosmetics, sunscreens, and is standardly used in sensitized solar cells.

Zeta potential analyzer

Titania's behavior at different pH's was similar to lead sulfide which the behavior is best represented in Figure 7 below. In Table 4 the average absolute value of zeta potentials increased as the pH increased. The pH value of 3.6 was dried and imaged based on the behavior of titania's isoelectric point. This zeta potential was as expected and was close to literature. The results for this material had some error to account for and had variance in multiple runs of the machine as shown for 9 pH for titania. If the particle size analyzer is correct as far as the measurements related to titania and lead sulfide, the particle measurements would be too large to achieve a nanoparticle haloing in the system. The reason there is doubt surrounding the instrument's readings is the

fact that powders are made of a large distribution of different diameters which this information is reflected in half width data points. The half width of the final run is an outlier to the data set similarly to lead sulfide quantum dots. For the same reason, the particle diameter will not be rejected since the it is likely the particle diameter could be included in the distribution. With a standard distribution of particle sizes available from the company of purchase, it could verify the true average particle diameter. Zeta potential measurements for 12.56 pH were similar for both lead sulfide and titania was why it ultimately was chosen to study further.

Table 4. Titanium dioxide zeta potential (mV) at different pHs

Titanium Dioxide Zeta Potential								
	pH							
Run	2	3	4	5	6	7	9	12.56
1	14.24	12.3	-8.475	-8.709	-22.98	-16.54	-41.61	-24.84
2	21.22	16.64	-11.02	-8.437	-22.42	-18.02	-46.35	-25.17
3	19.16	10.98	-10.35	-10.6	-28.88	-19.09	-40.06	-33.79
4	23.06	14.05	-15.23	-18.88	-24.43	-21.15	-36.27	-28.15
5	20.61	13.02	-12.96	-9.643	-22.78	-17.54	-32.39	-30.78
Mean	**19.66**	**13.40**	**-11.61**	**-11.25**	**-24.30**	**-18.47**	**-39.34**	**-28.55**
Standard Deviation	3.34	2.13	2.58	4.35	2.67	1.76	5.30	3.80
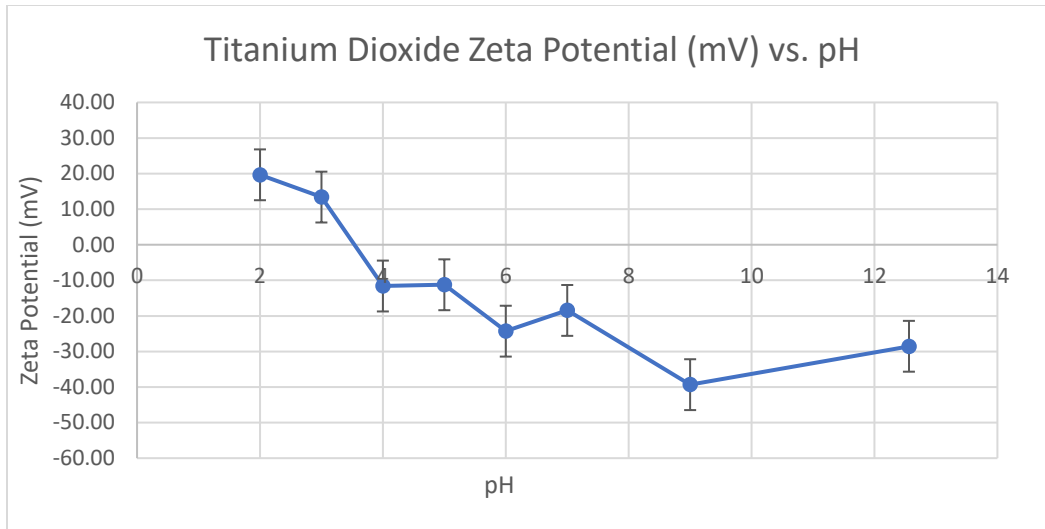
Figure 7. Graphical representation of mean zeta potential (mV) at different pHs. Graphed with one standard deviation error.

Particle size analyzer and SEM

Table 5. Particle Size Analyzer results in terms of effective diameter and half width.

Titanium Dioxide Particle Size Analyzer Results		
Run	Eff Diameter(nm)	Half Width (nm)
1	1608.8	1294.2
2	3841.9	4755.5
3	1597.2	1268.3
4	1696.3	1399.6
5	25	16.3
Mean	1753.8	1746.8
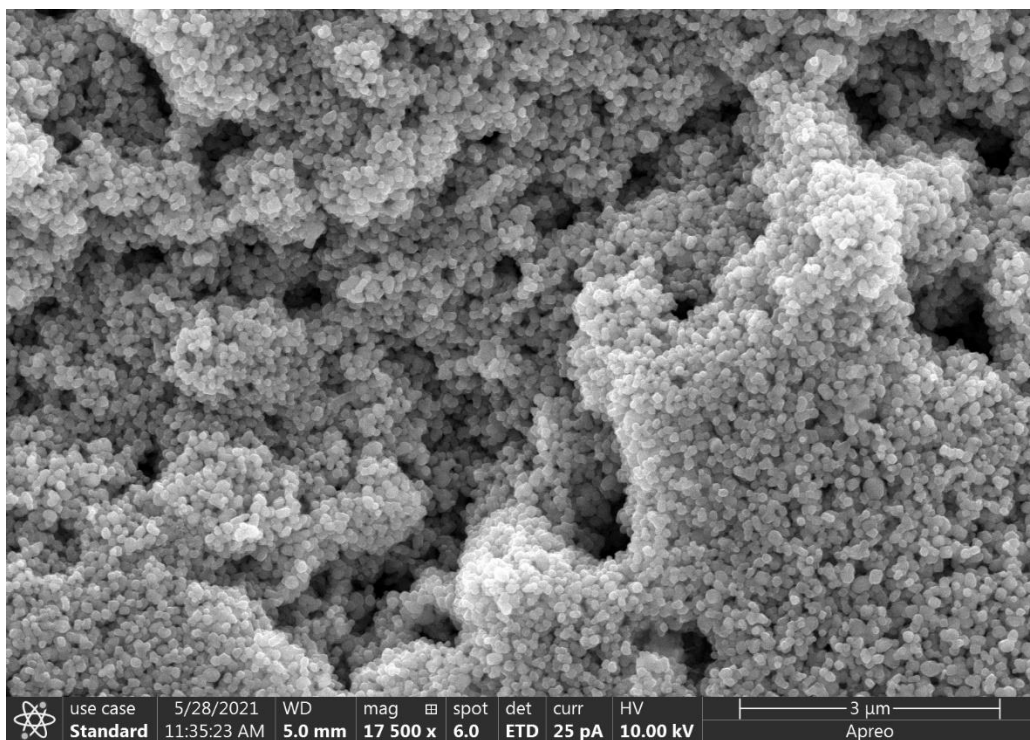
Figure 8. Titanium dioxide particles in a dried droplet structure.

Methods Overview

The general understanding of methods is to manufacture the quantum dots via colloidal synthesis. With these colloids in suspension, DSC-TGA analyzes the varying temperatures at which drying can occur as well as time frame for drying. By establishing the range of temperatures to test, we move to a larger scale via drying droplets in a standard lab oven controlling both time and temperature. Once a set of droplets have been dried, microscope pictures are taken to analyze the settling of particles in comparison to ambient temperature drying as well as access possible defects with varying temperatures.
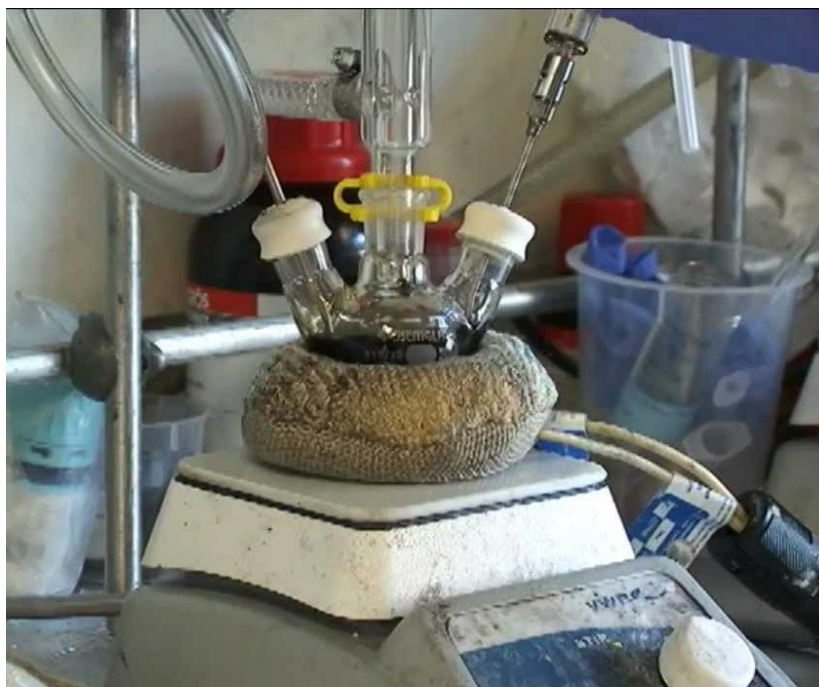
Figure 9. After addition of TMS and octadecene, the solution begins to form lead sulfide quantum dots.

The set up for the synthesis included 0.45 grams of granular lead into a 300-milliliter flask that is heated initially to 150°C in solution with Oleic Acid for 20 minutes under a nitrogen filled environment which is then increased to 173.4°C. Oxygen was purged from the system via a vacuum pump. The system was flushed three times by switching the vacuum and nitrogen feeds to ensure a pure nitrogen environment. Simultaneously, in another 300-milliliter round bottom flask 1-octadecene and bis(trimethylsilyl)sulfide (TMS) react. Once the solution in the lead and oleic mixture reaches 173.4 °C, an injection from the neighboring flask of TMS and octadecene is quickly added to the lead oleate mixture that has been created with heating. Once the addition occurs, the heating mantle is quickly removed and the solution is allowed to cool to room temperature while mixing to allow crystallization of PbS dots to form which

is occurring in Figure 9 above. Though literature suggested dissolving this solution in hexane and then precipitating the dots via methanol, this proved to be ineffective in removing the octadecene and oleate that remained. Removing and separating the dots was more difficult than anticipated after allowing the solution to evaporate overnight in the hood. It proved to not be effective (Hines & Scholes, 2003).

A suggestion from a research forum suggested creating a magnetic capture for the dots. Processing included dissolving the solution in hexane and placed small amounts of the target sample solution into a syringe that was packed with steel wool up to three milliliters in a five-milliliter syringe. Two strong magnets are taped to either side of the syringe to collect the dots. This, however, still presents a challenge of how to separate the excess oleic acid that cling to the particles. The other challenge being removing the quantum dots from the steel wool without losing a significant amount of product. Once these dots are isolated the solvent soaking the dots needs to be dissolved. Other solutions for removing the solvent that could have been attempted include utilizing a vacuum oven to evaporate the stubborn 1-octadecene. Ultimately it was chosen to leave the sludge like material on paper under a hood for a few weeks instead and the 1-octadecene seemingly evaporated in order to not contaminate another lab's oven. These materials were initially tested to see how the colloids behaved by air drying a small droplet on a glass slide.

Colloidal synthesis can develop its own error based off the reaction conditions. The temperature of the injection specifically effects the lead sulfide particle diameter. The higher the temperature of the injection gives a larger diameter. At 90 °C, the resulting particle size is 2.8 nanometers. At 120 °C, the particle diameter increases to

3.1 nanometers (Mousa, 2011). Another error that was experienced with this method is the materials were clumping together potentially due to surfactant which presents a challenge with imaging and achieving a nanoparticle haloing system.

Accument AB15 Plus pH Meter
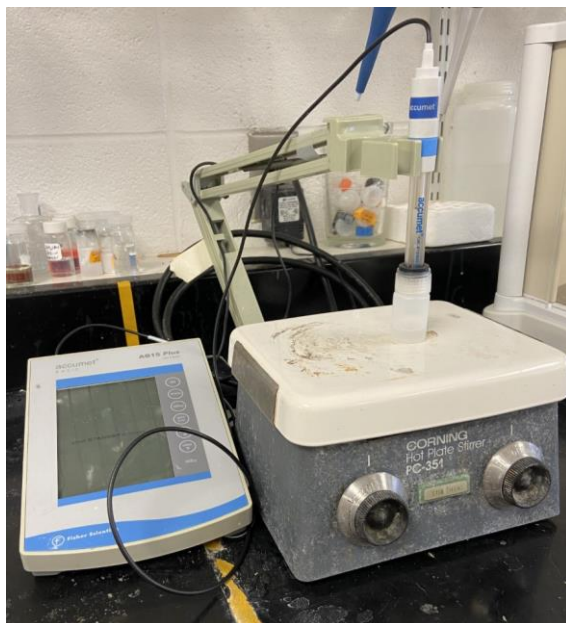
Figure 10. Picture of Accument AB15 plus pH meter with gel-filled polyer body pH combination electrode

The pH meter was used to measure not only the pH of samples containing the micro- and nanoparticle but also the solutions that are used to place samples into the zeta potential analyzer. In this case, after testing and assessing a microscopic picture with the different pH values, it was decided to test one above and one below on the pH scale. This applied for samples that included titanium dioxide and separately the lead sulfide quantum dots. Once data is arranged in tables assessing the zeta potential performance, pH is selected for the solution to assess the suspension performance.

Figure 11. Picture of Sonica Sonicator set up

To put together a suspension to be studied, dried PbS dots and TiO_2 particles are sonicated in a small glass vial surrounded in an ice bath after adjusting the pH of matrix solution. The sonicator was also used to suspend the single material vials to see the zeta potential and the overall charge of the particles in the solution. The stainless-steel tip was operated at a 20% amplitude.

Zeta Potential Analyzer/ Particle Size Analyzer

Zeta Potential Analyzer is used to measure the voltage of the suspension, and zeta potential, which is a measurement of the strength of a colloidal dispersion in a media. This analyzer measures the particle size as well as displayed in a graph. Samples are placed in cuvettes with about 1200 microliters, and after the probe is

rinsed with deionized water and dried then added to the cuvette. The cuvette with sample is placed into the analyzer to record the zeta potential in millivolts (mV) from using electrophoresis to the sample. This instrument is brought to temperature and reset between each measurement. These measurements are completed on the same sample. Zeta potential measurements will be inconsistent close to the isoelectric point. This is caused by the lack of stability of the solution due to zeta potential readings of 20 mV or less. Another error that can arise from zeta potential measurements is related to particle size.

The particle size analyzer is a part of the same instrument. To complete a particle size measurement, the cuvette is placed in the machine without the probe. The instrument uses light to measure the particles. This measurement is completed for a sample five times; each time the machine is resetting for the next run just like the zeta potential analyzer. With a large particle size, the materials will not achieve a nanoparticle haloing system. For large particle sizes to be more stable, it requires a higher pH which could not reflect what was expected.

Differential Scanning Calorimeter (DSC/TGA) Q20

Before drying materials and studying structure, materials were researched for their boiling point to establish a range of temperatures to test using Thermogravimetric analysis (TGA). TGA is a versatile analytical instrument that in this case was utilized for the ability to control ramping temperature and held isothermally (for standard) in a controlled atmosphere. The method's abilities include that of composition, thermal stability, phase transition, heat flow, and weight as a function of temperature.

In this instance, TGA measures various temperatures, recording both ramping temperatures up to 100 degrees Celsius. The purpose of conducting this analysis looks at the drying behaviors with higher temperatures of QDs in solution versus allowing the dots to dry in ambient conditions. TGA would mock these conditions by holding the temperature much like a solution being placed in a preheated lab oven being dried.

A part of the method was to physically inspect the solution once the sample had been analyzed which is somewhat of a disadvantage to using this method. If there were a way to flawlessly transfer the TGA dried samples to a lab dish to put under a microscope, it would significantly give a better understanding of how drying at higher temperatures affects the crystallization process. The overall process goals are to understand and produce crystallization while trying to avoid cracking and surface defects. Without this capability of seeing a profile image of a droplet drying from TGA, another way of assessing the crystallinity was by imaging and physical observation. TGA serves the purpose of establishing temperature ramping as well as isothermal understanding of the process of oven drying these samples.

Other methods considered included using a hot plate to view the materials as they dried however the drawback to this option is there are more factors that would need to be considered which is outside the scope of this project; Factors including variable humidity of the environment, assessing a proper temperature for the hot plate, and the ability to dry the material as quickly as possible. Drying the material with a hot plate would not be as beneficial as a standard lab oven because the glass slide would have to fully heat from the bottom to the top of the slide. A lab oven would dry a droplet faster by drying the glass in the direction of the heat in the oven to middle of the glass

slide relatively uniform in every direction. This transfer is relatively quick and reduces

the time it could take for the particles to settle out of suspension. With this analysis, a

standard lab oven was chosen over the alternative of heating a glass slide via hot plate.

Once heated imaging could be conducted with an optical microscope and SEM.

Zeiss Stemi 2000 Microscope and Fiber-Lite Fiber Optic Illuminator

Zeiss Stemi 2000 microscope established and confirmed the understanding of

drying and the overall mechanism of drying of a droplet on a glass slide. This

microscope's zoom range is 6.5x to 50x. Initial microscopic pictures were of ambient

dried quantum dots. The topics related to droplet drying are wetting dynamics, surface

tension, pressure, and the overall multiple structural collapses that inevitably occur

during drying. The process of drying and visually inspecting the slides at different

magnification on both sides of a microscopic glass slide gives the ability to inspect the

performance of the suspension. Visually inspecting the materials can be simplified via

plating dilutions.

Plating Dilutions

For this step, taking a dilution using a microplate as shown in Figure 12 below

which is typically used for biological dilutions for plating colonies. A 1:10 dilution

(original solution to new cell) was used since the dilution on a basis of 10 is an

uncomplicated conversion. Like biological samples, the more dilutions of a 1:10 basis

gives more distinguishable colonies to count. Techniques like biological sampling were

intuitive for creating clearer features and thinner layered droplets for SEM imaging. An

initial volume of 200 microliters is placed into the first cell and plated out to the third

dilution. Adjacent cells have the corresponding pH liquids with 180 microliters akin to

that of a broth medium. The process of dilution would be to take 20 microliters from the

pure sample and pipette it into the following cell. Swish around by quickly pipetting to

mix and then take 20 microliters and add to the next cell and so on. Once diluted,

imaging via SEM can be completed with defined structures.
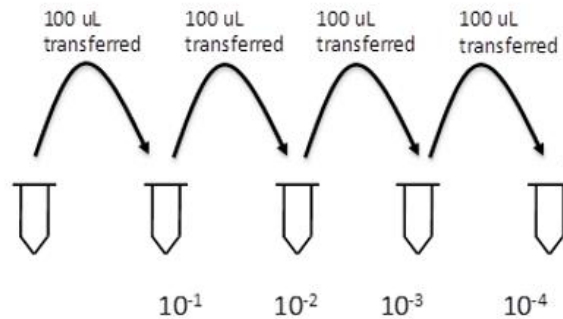
Figure 12. Example of dilution like cell culturing procedures used to dilute samples

Scanning Electron Microscope (SEM) : Thermo-Fisher Scientific Apreo C LoVac

FESEM

Scanning Electron Microscope captured the particle sizes of the dried quantum

dots. A beam of electrons from the electron gun is turned on in a vacuum chamber.

Electrons are deflected by a beam deflector through a lens. These electrons then

bounce off the specimen on the motorized stage and are reflected on to a detector.

Related to this study, T1 and ETD detectors are employed for providing close detailed

images of dried droplet samples of 0.1% titania and 0.01% lead sulfide; T1 detector has

the capability for materials differentiation (Mourdikoudis et. Al., 2018).
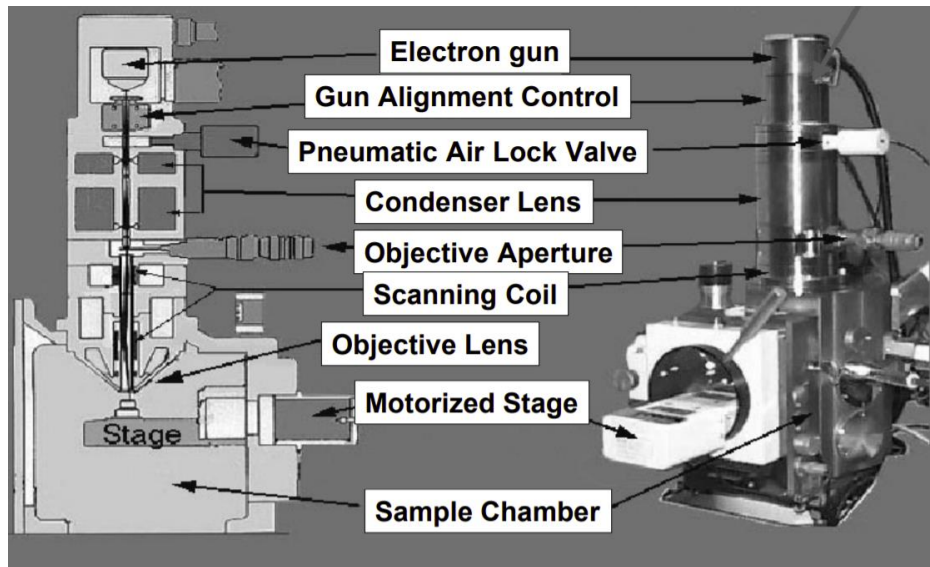
Figure 13. (top) SEM diagram from *"Electron Microscopy."; (bottom) image of SEM used for imaging at University of Louisville*

RESULTS & DISCUSSION

The overall approach to designing these sets of experiments were the

establishment of experimental conditions, preparation and understanding of solution

and material suspension, imaging of differing dilutions, and the drying and imaging of

samples and assessing their structure. To determine experimental conditions,

previously made solutions containing lead sulfide, titanium dioxide, and liquid media

(either potassium hydroxide, or nitric acid depending on pH), were assessed based off

known boiling points via thermogravimetric analysis to establish drying conditions. After

researching the evaporation temperatures of nitric acid and potassium hydroxide, 50,

60, 70, 80, 90, and 100°C drying temperatures were established as starting point for

TGA; these mediums were diluted which was considered when choosing starting point

temperatures. From the curves established by the TGA, the temperatures of 70, 80, 90,

and 100 °C were chosen as experimental temperatures with ambient drying conditions

as the control.

After synthesizing the lead sulfide quantum dots, the first step was to create

suspensions of our materials individually at different pHs to establish a zeta potential

profile and isoelectric point. Once these profiles were established, different

concentrations of quantum dots were tested to determined what would be best for

testing moving forward resulting in the two major sus of 1% PbS and 0.1% TiO_2, and

0.1% PbS and 0.01% TiO_2. Titanium dioxide in small amounts clouds a liquid media

very easily. From early tests, it was preferred to use 0.1% and 0.01% mixture to reduce

the waste of material as well as make sure the zeta potential could be determined with

no dilution. If solution is not opaque enough, the instrument will give error code

indicating that no measurement can be conducted. Below in Table 6 and Figure 14 are

the zeta potential measurements of lead sulfide and titanium dioxide. At lower pHs

these materials individually did produce a zeta potential that showed stability. As pH

increased above 10 pH for the PbS/TiO_2 mixture, the stability increased dramatically

above 30 millivolts. In terms of zeta potential, this result indicated a moderately stable

suspension. Considering the pH and the reduction of salt forming in drying, 12.56 pH

was chosen to reduce interference in SEM imaging with comparison to the 3.6 pH for

titania's isoelectric point. Once this profile and pH were determined using zeta potential,

initial ambient temperature drying of droplets on glass slides consisting of 10 microliters

were tested for drying behavior. The behavior of the materials with zeta potential are

questionable because of the error potentially associated with the particle sizes which

could explain the pH being stable at 12.56 versus the isoelectric point of titania.

Table 6. Zeta Potential (mV) of lead sulfide and titanium dioxide mixture at different pHs

Lead Sulfide + Titanium Dioxide (.01vol%, .1vol%)				
pH				
Run	5	7.3	10	12.56
1	-7.75	5.31	6.18	-37.13
2	-2.71	5.14	-5.29	-37.48
3	-7.15	-4.12	-6.28	-33.35
4	-6.35	2.28	-3.13	-38.94
5	-4.82	4.38	5.58	-37.14
Mean	-5.76	2.60	-0.59	-36.81
Standard deviation	2.02647	3.944137	6.017048	2.071755

After discussing imaging options for SEM, FTO (Fluorine-doped Tin Oxide) glass

was chosen to image droplets. In this case FTO glass was used but ITO (Indium Tin

Oxide) would have been just as suitable for the initial imaging. Imaging with SEM

confirms the concentration as well as how to get a profile view of a dried droplet. The

three ways that were tested were wax paper tabs, packing tape and scraping with a

razor blade as shown in Figure 15 below.
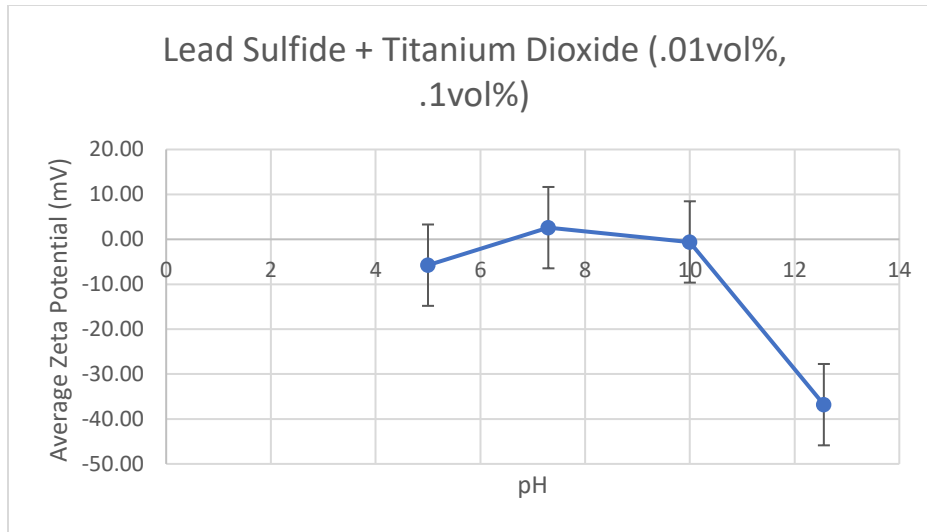
Figure 14. Graphed mean values for combined mixture of lead sulfide and titanium dioxide at each pH over the course of 5 measurements. Graphed with one standard deviation error.
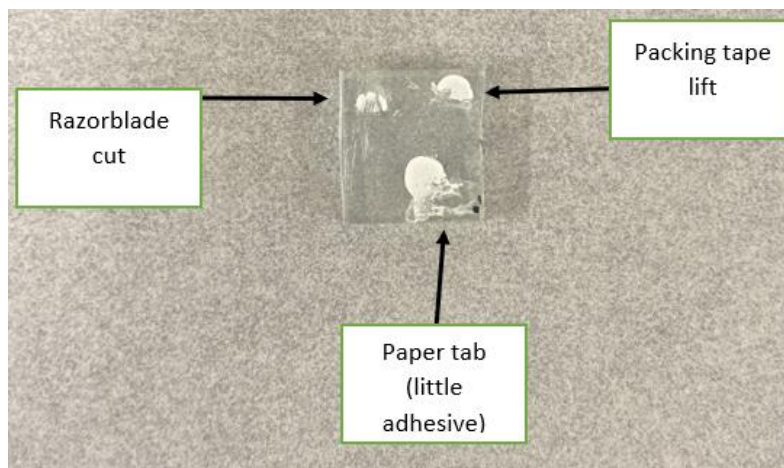
Figure 15. Different method testing of creating a profile view of a droplet

Based off imaging, packing tape provided the best as far as imaging. Razor blade cuts resulted in streaking on the glass. Packing tape provided a very clear cut as far as residue left on the slide but was not as helpful because the cut did not give a perfect profile view. Paper tabs were the least effective from streaking, crystallization, and smudging; it was not an effective method from the lack of being able to assess the final structure. Conclusions of this imaging session were to shrink the droplet size as

well as dilute concentrations of materials to increase visibility of the droplet profile. After a subsequent imaging session that in order to achieve a profile view of a droplet, the best method would be to place a droplet as close as possible to the edge of the glass.

Utilizing a biological dilution plate, samples were diluted using 1:10 dilution in corresponding cells. Much like a standard procedure for plating and counting biological colonies, a 100% concentration (200 microliters) of our original sample was placed in the first cell. The next 5 cells were filled with the corresponding pH of the sample's solution (180 microliters). 20 microliters are taken from the 100% concentrated cell and placed into the adjacent cell. This is pipetted and swished to make sure there is a good distribution of material in the new cell. After testing some DI water, the droplet size was reduced to 2 microliters to ensure a small enough drop.

These solutions were diluted, dried, and imaged to determine what dilution gives the thinnest and clearest 45-degree profile image on the SEM. The imaged results are in Figure 16 below. The option that gave the clearest and visually pleasing image was the third dilution of 1:10, represented as 10^{-3}. The first, top left, image was a profile of a droplet and shows the dense amount of dried material that is too dense to see visually differentiate between lead sulfide and titania. After another dilution of the materials, the droplet was opaque and shows some white crystals starting to show through; crystals that are appearing are fluoride-doped tin oxide in the glass substrate. Finally, the third dilution had structures that visually could be identified based off the thin layer that was created during drying. In this case, seeing these small holes showing white crystals indicates that the layer is thin enough. When the layer is too thick it creates dark canyon like structures that appear in more dense solutions which produces dark

crevices like in Figure 16 on the top right. It can be speculated that these are dark

canyons are lead sulfide QDs but that claim is not definitive without thinning out the

layer in an attempt to clarify understanding.
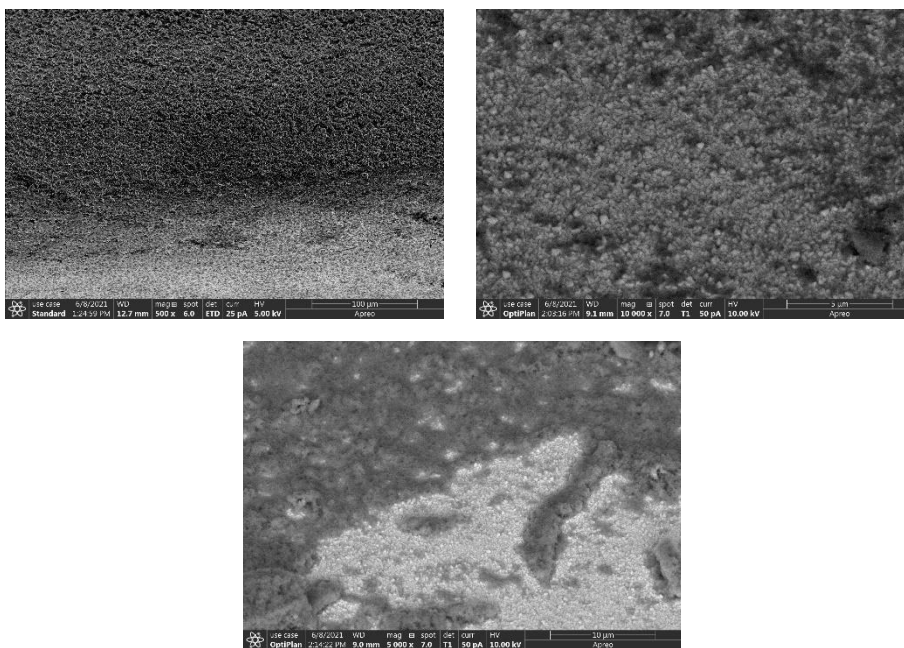
Figure 16. first 1:10 dilution(10^{-1}) profile view of droplet (top left), second dilution (10^{-2}) top surface view of droplet(top right), third dilution (10^{-3}) top view of droplet edge (bottom).

Once this round of imaging was completed it was determined that the FTO glass was

beginning to interfere with imaging by showing up as little bright crystals as shown in

Figure 17. This result of imaging was inconclusive in defining material behavior. After

discussing with some of the staff in the technology center, a silicon wafer would produce

images that did not create interference like FTO glass. When imaging was completed

with the diluted material and properly adjusting the droplet placement close to the edge

of the silicon wafer, the diluted droplet profiles were obtained using a 45-degree angle

SEM sample loader. On each wafer there are two dots which contain a sample of

42

materials at 3.6 and 12.56 pH. 3.6 pH representing the approximated isoelectric point of

titanium dioxide which was determined in our initial materials characterization. In Figure

18 below the profile views were not conclusive. The reasoning being dark matter while

having high magnification cannot be completely characterized. The dark material

displayed could be organic matter that has clung to the surface of the wafer or the

quantum dots being repelled from titania. Additional images were collected of the top

surfaces of the dried droplet which was analyzed following not having the ability to have

a definitive conclusion from profile images.
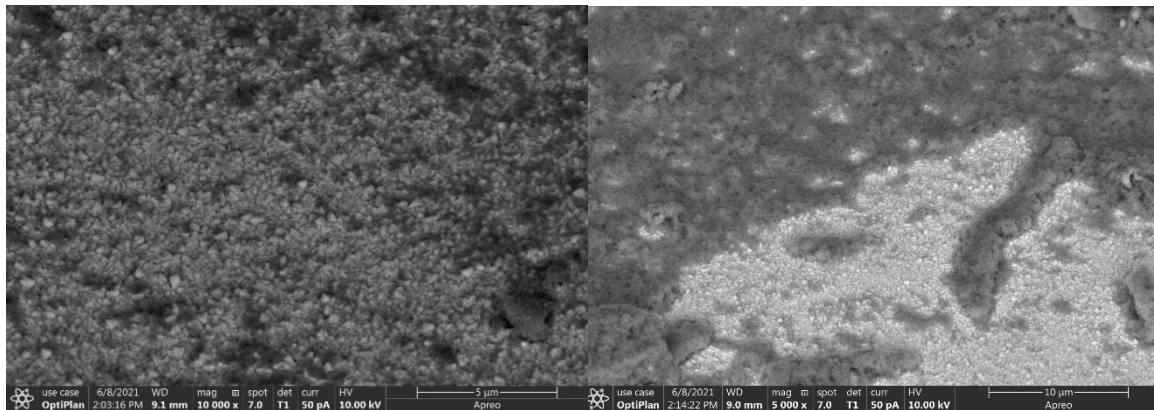
Figure 17. T1 detector on SEM showing interference (small little white crystals) created by flourided doped tinoxide(FTO) glass.
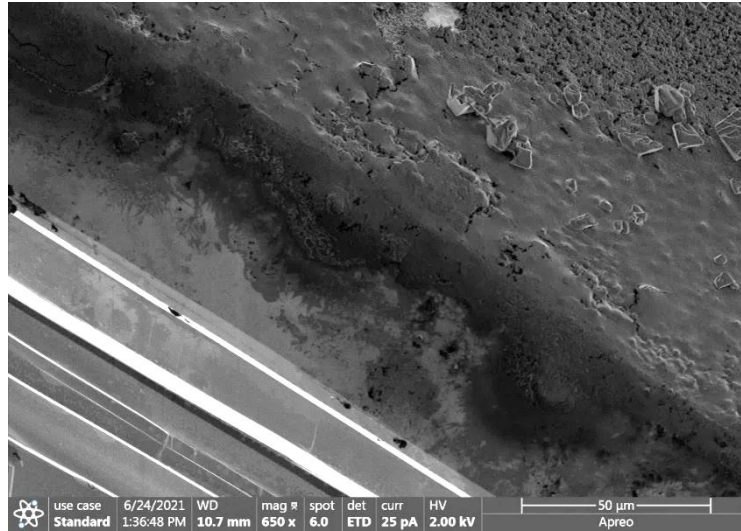
Figure 18. Profile views using SEM. Conditions of drying: 70 degrees Celsius, on silicon wafer.

In Figure 19 drying droplets demonstrated a distinct separation of materials but this is not true for all samples provided in the figure. In images captured by the SEM, it appears a bright material is surrounded by a dark body. Intuitively the bright material being titania and the darker ring being quantum dots. Presumed conclusions, preferably, needed to be further verified. The images with gray scale materials on the left column of the figure were taken to a higher magnification and showed separation.

Again, the imaging showed a lighter material, presumed to be titania, surrounded with dark edges, presumed quantum dots. The challenge with these images is that a profile image did not provide the expected outcome with a silicon wafer.

Challenges that arise with 12.56 pH samples is the formation of a crystal layer or crystal bodies which can be seen in some of the samples; crystal layer on the surface of the dried material results in inability to observe material definition using ETD or T1 detectors. These salt crystals are from potassium hydroxide used to achieve higher pHs for zeta potential characterization. Using a backscatter detector for this purpose would not be of help because this detector operates in gray scale and does not give a clue as to materials composition of the droplet profile. With a T1 detector, which assesses the materials in a sample, it is difficult to distinguish between the two because images appear darker for materials further down the periodic table. With titanium and lead being close together on the periodic table, this detector does not have the ability to register an image that can differentiate between materials.

While this imaging was still accomplished, another avenue of determining the overall drying effects had to be employed; SEM images did not provide definitive proof of how the droplets were drying or the desired profile view. Silicon wafers are not translucent; therefore, glass slides were used to look at both sides of a dried droplet to potentially assess how the particles were behaving. The combination of SEM imaging and microscopic imaging can bridge or explain visually what is occurring.
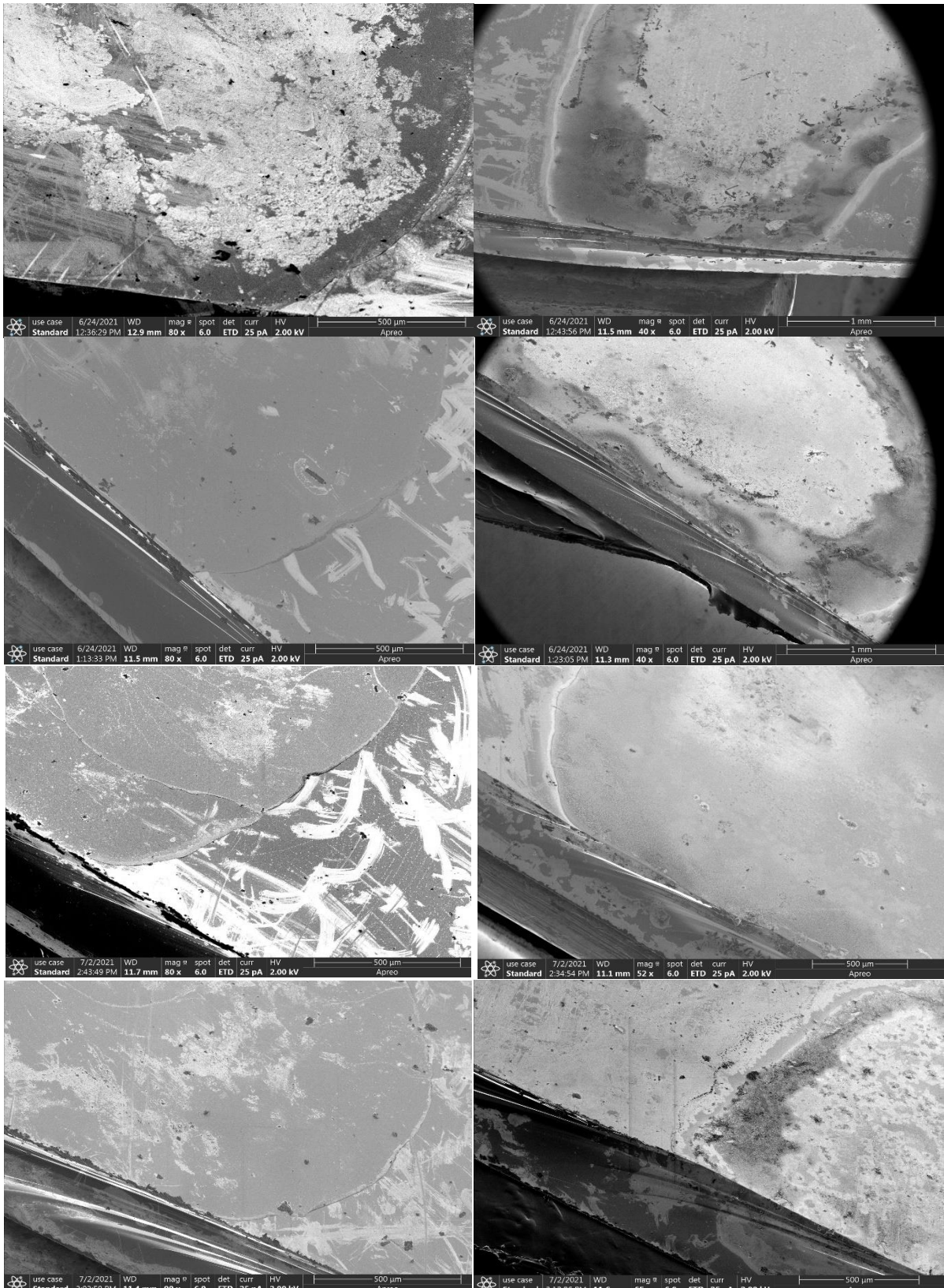
Figure 19. SEM images captured of 70 (row 1), 80(row 2), 90 (row 3), and 100 (row 4) degrees Celsius. These temperatures were tested on colloidal suspensions at 3.6 (left column) and 12.56 (right column) pHs.

Using a lab oven, droplets were dried. First the droplet face side of the glass was inspected and then the opposite side of the glass in an optical microscope. Imaging finally brought some clarity of how the droplets were drying as shown in Figure 20. Below the left image shows a primarily white surface which is majority of the titanium particles with a faint gray outer ring (lead sulfide) confirms SEM imaging results in Figure 19; while the right image shows a darker, more gray color to the bottom face of the droplet. What is occurring is the materials are settling and falling out of suspension. The quantum dots are falling to the bottom as the titania remains on the top surface. This process was repeated for all temperatures at 3.6 and 12.56 which all slides resembled that of Figure 20 and are presented in Figure 21 and Figure 22. Thus, supporting results that confirm the materials are falling out of suspension with titanium dioxide on the top surface interface and lead sulfide settling to the bottom.

The issue with the images Figure 21 and Figure 22 is that the images show darker clumps of particles which is the lead sulfide. With this microscope, these dots should not be visible. While distributed on the bottom relatively evenly, seeing the particles is the most important issue. These lead sulfide particles are clumping together since they are visible in these images. This, however, would need to be confirmed with a particle shape analyzer to determine clumping behavior in solution in the liquid phase.

47
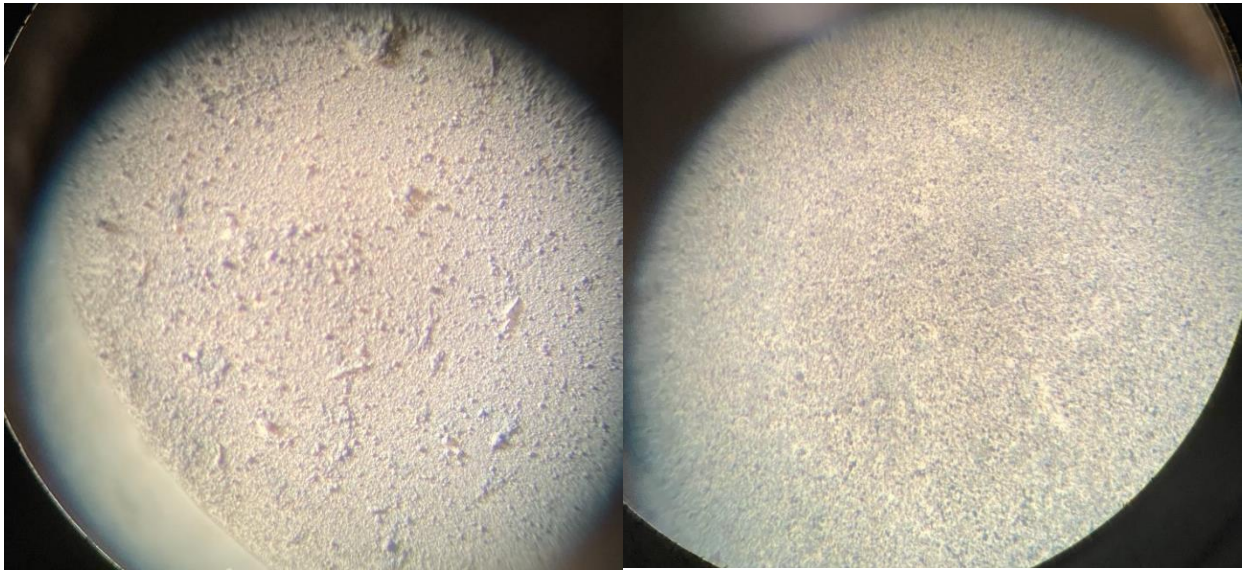
Figure 20. (left) Image captured of droplet face side by IPhone through microscopic lense on Zeiss Stemi 2000 Microscope and using the Fiber-Lite Fiber Optic Illuminator at 30X; (right)backside of glass microscope slide 50X

3.6 pH   12.56 pH

Figure 21. Microscopic slide pictures with each set representing the front and back of a sample at given temperature. First row are samples dried at 70 °C. Second row dried at 80 °C. 30X, and 50X (top left set); 25X, and 30X (top right set); 30X, and 50X (bottom left set); 30X, and 50X (bottom right set)

49

3.6 pH   12.56 pH

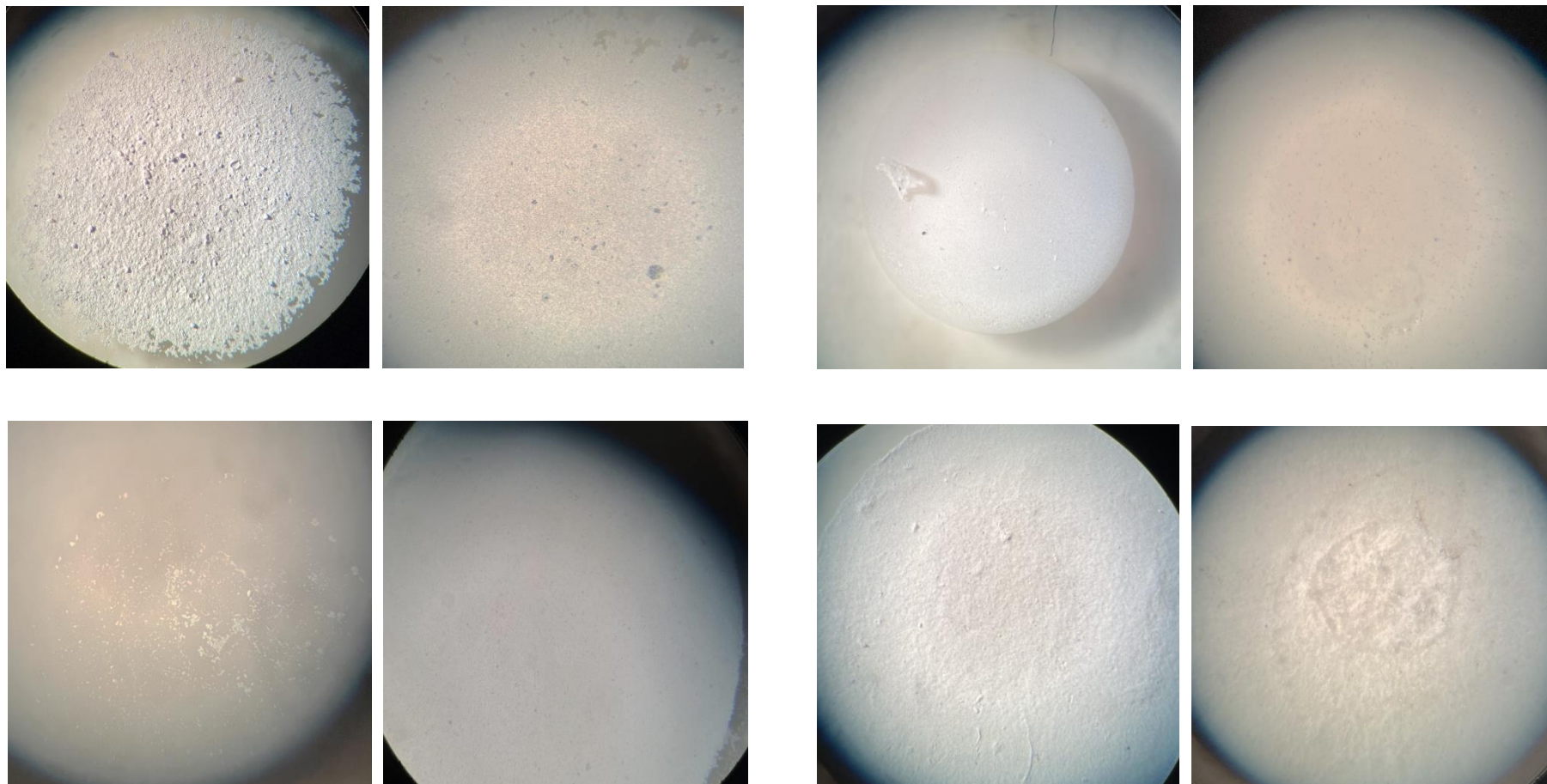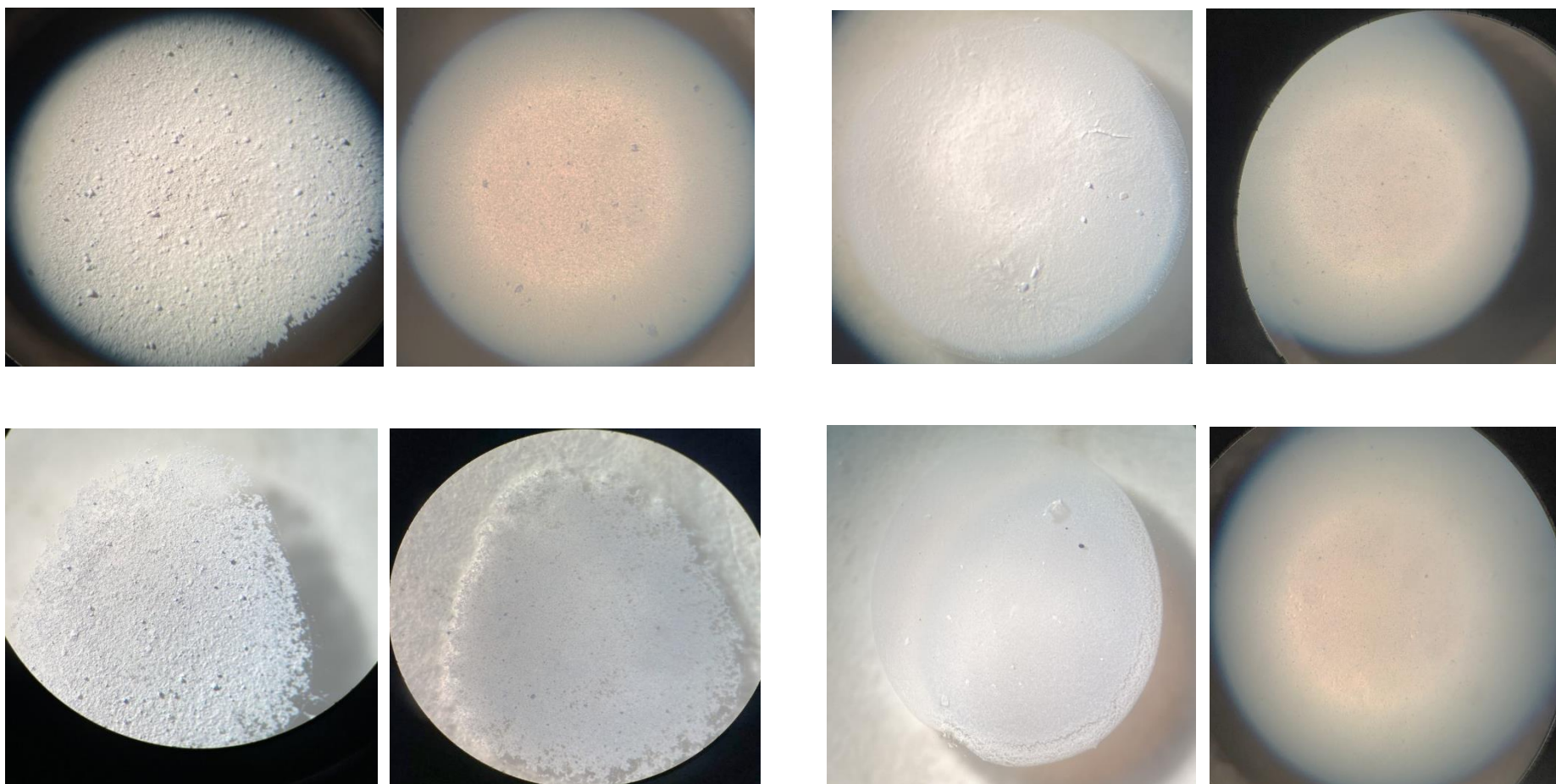
Figure 22. Microscopic slide pictures with each set representing the front and back of a sample at given temperature. First row are samples dried at 90 °C. Second row dried at 100 °C. 30X, and 50X (top left set); 20X, and 30X (top right set); 20X, and 25X (bottom left set); 20X, and 30X (bottom right set)

Sources of Difficulty, Error, Explanation, and Looking to the Future

The question that arises from this result is what could be causing this separation of materials and what can be done to reduce or prevent the suspension in materials from falling out? There are a few explanations that could explain why this phenomenon is occurring including: particle size distribution of materials, the behavior of materials regarding charge, and lead sulfide colloidal synthesis method. If the particle size analyzer is correct as far as the measurements related to titania and lead sulfide, the particle measurements would be too large to achieve a nanoparticle haloing in the system. The reason there is doubt surrounding the instrument's readings is the fact that powders are made of a distribution of different diameters. While the results present an average diameter of particles, the half width is a large value meaning the distribution is large. Particle size analyzers present their own challenges related to measuring particle diameter. If assessed by a particle shape analyzer and sieving by particle size, it could confirm whether particles are clustering together and have a more accurate particle distribution size with images to further understand material behavior.

As referenced from the initial materials characterization, both materials require a very high pH to maintain suspension. Since the materials are of the same charge, once mixed as time passes it starts to separate. The separation is occurring because the materials are repelling each other due to the negative charges. This in part could be caused by larger particle size resulting in a higher pH to keep the materials in suspension. Looking forward, it should be assessed if and how this system could be

changed to create nanoparticle haloing by having a positive and negatively charged materials.

Lead sulfide colloidal synthesis method could be to blame for the charge creating a negative charge. The chosen method could be leaving negative ions charging the material via bis(trimethylsilyl)sulfide as known as TMS. When performing the colloidal synthesis, the material after was hard to wash. Used a variety of solvent to try to pry from the quantum dots to clean them. The yield was low using this method. In the future another method of performing the colloidal synthesis should be considered as well as potentially buying the dots beforehand with confirmation and guarantee of particle size.

CONCLUSION

Lead sulfide quantum dots and titanium dioxide are studied for wetting and drying effects. Methods employed to acquire results include a pH meter, particle size analyzer/zeta potential analyzer, microscopic imaging, and SEM imaging. Zeta potential, pH values, SEM, and microscopes were ways of quantifying or observing the colloidal suspension and dried sample behavior. Conclusions from zeta potential measurements showed individually tested materials stabilized at pH around 12.56. A variety of pH values were used to characterize behavior related to zeta potential of individual and combined materials. Combined mixtures of lead sulfide and titania were dried at two pH values. Titania's isoelectric point was at 3.6 pH; a mixture at 12.56 pH was tested because of the observed zeta potential behavior showed increased stability occurring. As well a nanoparticle haloing system would occur ideally when there is increased stability of the quantum dots at the isoelectric point of titania. This did not perform as expected from prior understanding of lead sulfide's behavior at 3.6 pH.

From these conclusions, SEM imaging technique was optimized to achieve a thin layer of dried material to see how the material drying behavior. Images for SEM appeared inconclusive from a profile view of a droplet, but it was observed that in some images there was a separation of material visible; sample observations needed to be further verified using another method of imaging. Optical microscope imaging further confirmed what was occurring in SEM imaging; the materials were falling out of suspension with lead sulfide settling to the bottom and sides, and titania on the top surface of the dried droplet.

Initial solar cells utilized silicon and alloys for their economic viability. Photoelectrochemical photovoltaic cells were discovered with technological advancement which increased solar efficiency and further improved economic feasibility. This work completed further establishes behavioral evaluation of individual materials related to creating third generation solar devices made with quantum dots verses that of current materials used for second generation materials like CdS, CdSe, and CdTe. It confirms that lead sulfide particles as a nanoparticle need to be evaluated on multiple levels. This work refutes the prior idea that this colloidal synthesis method is appropriate to use. For future research, it brings into question if the materials should be purchased prior due to the surfactant material clinging to the particles and causing clumping in the imaging in Figure 21 and Figure 22. The materials themselves have a large particle diameter and need to be further characterized outside the scope of this project. Additionally, this material synthesized in the lab brings into question whether a nanoparticle haloing system is viable with lead sulfide materials as previously thought \.

It brings into question the viability of proceeding with lead sulfide for studying

nanoparticle haloing systems.

REFERENCES

Averill, B., & Eldredge, P. (2019). Chemistry: Principles, Patters, and Applications.

https://chem.libretexts.org/Bookshelves/General_Chemistry/Book%3A_Chemistry_(Averill_and_Eldredge)

Bhuiyan, M. H. U., et al. (2015). "Effect of Nanoparticles Concentration and Their Sizes on Surface Tension of Nanofluids*." Procedia Engineering* 105: 431-437.

https://www.sciencedirect.com/science/article/pii/S1877705815008279

"Electron Microscopy." Retrieved July 1,

2021.http://web.pdx.edu/~pmoeck/phy381/Topic3B-SEM-Total.pdf

Harikrishnan, A. R., Dhar, P., Gedupudi, S., & Das, S. K.. (2017). Effect of Interaction of Nanoparticles and Surfactants on the Spreading Dynamics of Sessile Droplets. *Langmuir*, 33(43), 12180–12192. https://doi.org/10.1021/acs.langmuir.7b02123

Hines, M. A., & Scholes, G. D. (2003). Colloidal PbS Nanocrystals with Size-Tunable Near-Infrared Emission: Observation of Post-Synthesis Self-Narrowing of the Particle Size Distribution. Advanced Materials, 15(21), 1844-1849.

https://doi.org/https://doi.org/10.1002/adma.200305395

Jasim, K. E.. (2018). Lead Sulfide Quantum Dot Sensitized Nanocrystalline Solar Cell. *Kne Engineering*, *3*(7), 171. https://doi.org/10.18502/keg.v3i7.3081

Kouhnavard, M., Ikeda, S., Ludin, N. A., Ahmad Khairudin, N. B., Ghaffari, B. V., Mat-Teridi, M. A., Ibrahim, M. A., Sepeai, S., & Sopian, K. (2014). A review of semiconductor materials as sensitizers for quantum dot-sensitized solar cells. Renewable and Sustainable Energy Reviews, 37, 397-407.

https://doi.org/https://doi.org/10.1016/j.rser.2014.05.023

 NPR Newswire. (2020). "Global Quantum Dots Report 2020-2030: A Potential Market Value of $35+ Billion." Retrieved May 24, 2021, from

https://www.prnewswire.com/news-releases/global-quantum-dots-report-2020-2030-a-potential-market-value-of-35-billion-301152096.html.

Mourdikoudis, S., Pallares, R. M., & Thanh, N. T. K.. (2018). Characterization techniques for nanoparticles: comparison and complementarity upon studying nanoparticle properties. Nanoscale, 10(27), 12871–12934.

https://doi.org/10.1039/c8nr02278j

Mousa, A. (2011). Synthesis and Characterization of PbS Quantum Dots. *Lunds Universitet.*

Osman, A., et al. (2017). "Fundamental Investigation of the Drying of Solid Suspensions." *Industrial & Engineering Chemistry Research* **56**(37): 10506-10513.

Sigma Aldrich. (2021). "Quantum Dots." Biosensors & Bioimaging. Retrieved May 30, 2021, from https://www.sigmaaldrich.com/US/en/technical-documents/technical-article/materials-science-and-engineering/biosensors-and-imaging/quantum-dots .

Tohver, V., Smay, J., Braem, A., Braun, P., and Lewis, J. (2001). Nanoparticle halos: A new colloid stabilization mechanism. PNAS 98: 8950-8954

Raja, P. M. V., & Barron, A. R. (2021). Book: Physical Methods in Chemistry and Nano Science. https://chem.libretexts.org/@go/page/55670

CURRICULUM VITA

NAME:

Kelly Marie Lee

ADDRESS:

Department of Chemical Engineering

216 Eastern Pkwy

University of Louisville

Louisville, KY 40208

DOB:

Houston, Texas – August 28, 1995

EDUCATION & TRAINING:

B.S., Chemical Engineering

University of Louisville

2014 -- 2018